Interdiffusion in Heusler film epitaxy on GaAs(001)

C. Gusenbauer,[1] T. Ashraf,[1] J. Stangl,[1] G. Hesser,[2] T. Plach,[2] A. Meingast,[3] G. Kothleitner,[3] and R. Koch[1]

[1] *Institut f. Halbleiter- und Festkörperphysik, Johannes Kepler Universität, Altenbergerstrasse 69, A-4040 Linz, Austria*

[2] *Zentrum für Oberflächen- und Nanoanalytik, Johannes Kepler Universität, Altenbergerstrasse 69, A-4040 Linz, Austria*

[3] *Institute for Electron Microscopy, Graz University of Technology, Steyrergasse 17, 8010 Graz, Austria*

(Received 19 August 2010; published 24 January 2011)

We report the role of interdiffusion in molecular beam epitaxy of the binary Heusler alloy system $Fe_{1-x}Si_x$/GaAs(001), employing a variety of complementary techniques that, in their combination, provide quantitative insight into the dynamics of the involved processes. The main properties of the investigated $Fe_{0.84}Si_{0.16}$ and $Fe_{0.76}Si_{0.24}$ films—growth, epitaxy, crystallographic order, interface quality, saturation magnetization, coercive field, and magnetic anisotropy—are in perfect agreement with the literature. Additionally, our results reveal a strong interdiffusion of Fe and Si into the GaAs substrate as well as of As and Ga into the $Fe_{1-x}Si_x$ films, creating intermixed layers of 2–3-nm thickness in both film and substrate. Interdiffusion is dominant already at moderate growth temperatures required for crystallographic ordering, thus demanding new concepts including appropriate diffusion barriers for the development of ferromagnet/semiconductor hybrid systems.

DOI: 10.1103/PhysRevB.83.035319 PACS number(s): 68.35.Fx, 68.35.Gy, 68.35.bd

I. INTRODUCTION

Ferromagnetic layers with a high spin polarization on semiconductor substrates are attracting increasing interest as potential spin injectors for spintronics[1] or magnetoresistive elements for magnetoelectronic devices.[2] High spin-polarization materials commonly are binary or ternary transition-metal compounds such as certain FeCo alloys[3] and Heusler compounds (e.g., Fe_3Si or Co_2FeSi). According to theory,[4] for the latter material class, perfect crystallographic order is essential for attaining high spin polarization. Furthermore, for efficient spin injection the interface has to be abrupt and, even more annoying, it seems to depend dramatically on the type of atoms that participate in the contact layer to the substrate.[5] Consequently, interface disorder due to interdiffusion or interface reactions between film and substrate is detrimental for technological application. Recently Ramsteiner *et al.*[6] discovered that during deposition of Co_2FeSi onto GaAs(001) Co, Fe, and Si diffuse about 50 nm deep into the substrate by a thermally activated process. Since the metal atoms may act as paramagnetic spin-scattering centers, the obtained spin injection is low, even though excellent abrupt interfaces have been revealed by high-resolution transmission electron microscopy (HRTEM).[7]

Here we report on interdiffusion processes occurring during molecular beam epitaxy (MBE) of binary, thus experimentally simpler $Fe_{1-x}Si_x$ films on GaAs(001). The composition of the films is in the range of the Heusler compound Fe_3Si with $x = 0.25$ (Fig. 1). We employed a variety of complementary experimental techniques that—in their combination—provide quantitative insight into the dynamics of the ongoing interdiffusion processes: (i) *in situ* stress measurements as a real-time technique for monitoring film growth[8] and interdiffusion;[9] (ii) a calibrated quartz crystal microbalance (QCM) to directly measure the mass equivalent of deposited Fe and Si for determining film thickness and composition; (iii) x-ray diffraction (XRD) for investigation of structural order and the thickness of the crystallographically ordered layers; (iv) cross-sectional HRTEM for obtaining real-space information on epitaxial growth, crystallographic order, film thickness, and interdiffusion; (v) reflection high- and low-energy electron diffraction (RHEED and LEED) as well as atomic force microscopy (AFM) for investigating surface structure and morphology; (vi) a cantilever beam magnetometer (CBM)[10] for quantitative magnetization measurements; (vii) Auger depth profiling; and (viii) scanning transmission electron microscopy (STEM) in combination with energy dispersive x-ray spectroscopy (EDXS) to detect, identify, and localize interdiffusing species. Our study reveals considerable diffusion of Fe and Si into the GaAs substrate as well as of As and Ga into the $Fe_{1-x}Si_x$ films, creating intermixed layers of 2–3-nm thickness in both film and substrate. Diffusion increases with the growth temperature and is dominant already at typical temperatures necessary for crystallographic ordering. Moreover, our study discloses fundamental difficulties in determining the correct composition of binary and ternary compounds prone to interdiffusion from the XRD data, since in that case a direct comparison of the XRD lattice constants with respective bulk constants is not applicable.

The paper is organized as follows: After a short experimental description in Sec. II, the results on two types of $Fe_{1-x}Si_x$ films, $Fe_{0.84}Si_{0.16}$ and $Fe_{0.76}Si_{0.24}$, will be presented in Sec. III and discussed in the context of the current literature. The paper is concluded by a summarizing discussion in Sec. III F.

II. EXPERIMENTAL

The experiments were performed in a multichamber ultrahigh vacuum (UHV) system consisting of separate interconnected growth chambers for III/V semiconductor and metal MBE. The $Fe_{1-x}Si_x$ films were deposited onto $c(4 \times 4)$ reconstructed GaAs(001) cantilever-beam substrates prepared in the III/V growth chamber by standard GaAs techniques (low-temperature buffer growth at 480 °C, high-temperature buffer growth at 590 °C, annealing at 605 °C, controlled cooling to 380 °C at constant As_4 flux to form the $c(4 \times 4)$ reconstruction followed by further cooling at reduced As_4 flux). The $c(4 \times 4)$ reconstruction is maintained during sample transfer into the metal growth chamber as checked by RHEED and LEED.

 ©2011 American Physical Society

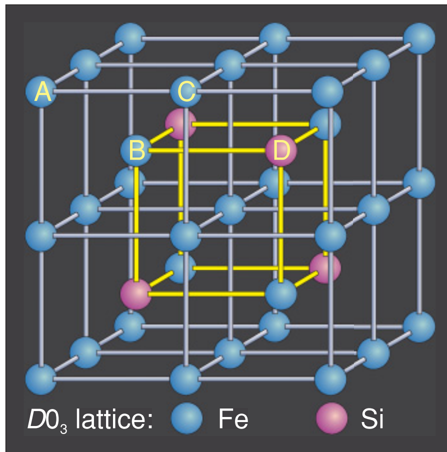

FIG. 1. (Color online) Sphere model of the $D0_3$ lattice of Fe_3Si: It consists of a regular array of body-centered cubes where the corners (A, C) are occupied by Fe atoms and the center atom is alternatingly Fe (B) or Si (D).

The $Fe_{1-x}Si_x$ films were deposited at a pressure of 8×10^{-10} mbar and a Si deposition rate of 0.05 nm/min. The Fe deposition rate was adjusted appropriately between 0.5 and 1.5 nm/min according to the respective $Fe_{1-x}Si_x$ composition. The deposition rates of Fe and Si were measured and controlled by a quartz crystal microbalance (QCM) calibrated by a QCM in substrate position. From the obtained mass equivalent of deposited Fe and Si composition and nominal thickness of the $Fe_{1-x}Si_x$, films were calculated. A CBM[10] was used for measuring the stress of the $Fe_{1-x}Si_x$ films in real time during growth as well as their magnetic properties *in situ* after the deposition.

The XRD and HRTEM investigations were performed *ex situ* with a Seifert XRD3003 and a JEOL-2011 TEM, respectively, the AES investigations with a JEOL-JAMP-9500F field emission Auger microprobe. The STEM-EDXS investigations were carried out by a FEI Tecnai F20 electron microscope equipped with an Si(Li) EDX detector from EDAX. Prior to the EDXS-measurements the specimens were oriented into the GaAs[110] zone axis and specimen drift was corrected before each measuring point of a EDXS linescan. To guarantee appropriate resolution and sufficient beam current, a STEM full-width-at-half-maximum beam size 0.36 nm was chosen. For the estimated specimen thickness of ≈50 nm the electron beam spread is negligible (with only 1% of the electrons being outside of the nominal beam diameter in GaAs), leading to an overall measurement resolution of 0.5 nm.

III. RESULTS

Growth, structure, and magnetic properties of $Fe_{1-x}Si_x$ films on GaAs(001) with compositions close to that of the Heusler compound Fe_3Si have been studied intensively in previous years.[11–17] Structure and magnetic properties of our $Fe_{1-x}Si_x$ films prepared with two compositions, $Fe_{0.84}Si_{0.16}$ and $Fe_{0.76}Si_{0.24}$, as determined by QCM, are in excellent agreement with these studies. We remark, however, that in order to enhance sensitivity toward interdiffusion effects our films are significantly thinner (~7 nm versus typically 20–50 nm).

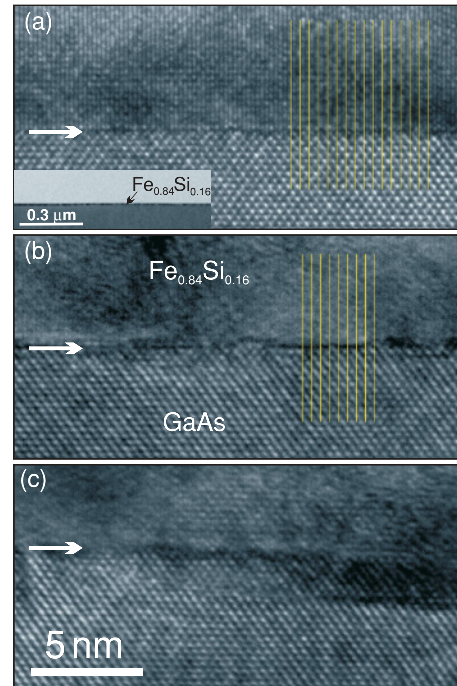

FIG. 2. (Color online) High-resolution TEM images along [110] of the interface region of $Fe_{0.84}Si_{0.16}$/GaAs(001): (a) $T_G = 150\,^{\circ}C$, (b) 200 °C, (c) 250 °C. Vertical lines illustrate pseudomorphic growth and arrows mark interface. Inset shows a larger section of the 150 °C film.

A. Growth and structure

All films of this study have grown epitaxially with an in-plane lattice spacing equal to that of GaAs(001) as evidenced by HRTEM [e.g., Figs. 2(a) and 2(b) and azimuthal XRD scans (not shown)]. In agreement with the literature, the optimum growth temperature (T_G) turns out to be a tradeoff between realizing good crystallographic order according to the $D0_3$ lattice (i. e., high T_G)[15] and avoiding interdiffusion and chemical reactions at the interface (i. e., low T_G).[17] The compromise is found at $T_G \approx 200\,^{\circ}C$.[12,15] Figure 3 shows

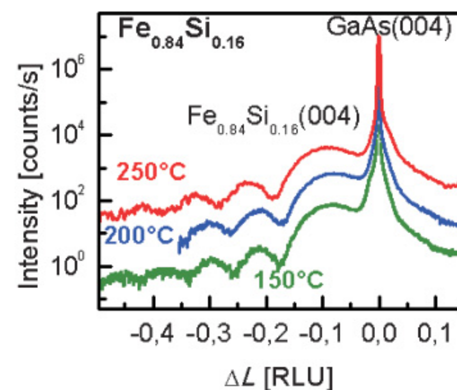

FIG. 3. (Color online) XRD spectra (intensity versus relative x-ray momentum change in reciprocal lattice units) of $Fe_{0.84}Si_{0.16}$ films on GaAs(001) deposited at 150 °C, 200 °C, and 250 °C. In addition to the (004) reflection of the $Fe_{0.84}Si_{0.16}$ films, pronounced thickness oscillations are observed at all growth temperatures pointing to a good surface and interface quality.

XRD spectra of the $Fe_{0.84}Si_{0.16}$ films deposited at different growth temperatures. The out-of-plane (004) reflection of the $Fex_{0.84}Si_{0.16}$ films appears at smaller angles than the respective GaAs peak, thus indicating an expanded lattice in the vertical direction and accordingly a compressively strained lattice in the film plane. In agreement with Herfort *et al.*,[12] pronounced thickness oscillations (Pendellösungen) are observed that point to smooth and abrupt interfaces at T_G of 150–250 °C. However, the cross-sectional HRTEM images of Fig. 2 reveal an abrupt interface with a thickness at the absolute minimum of 1–2 ML (monolayers) only for the 150 °C film [Fig. 2(a)]. At $T_G = 200\,°C$ the transition region between film and substrate broadens to 2–3 ML with distinct steps of lattice-distance height visible in TEM images [Fig. 2(b)]. At $T_G = 250\,°C$ the interface degrades further exhibiting a roughness of 2–3 nm [Fig. 2(c)]. Figure 4(a) includes the (004) spectra of a $Fe_{0.76}Si_{0.24}$ film deposited at 200 °C. The film reflection is shifted closer to the corresponding GaAs peak indicating a decrease of the unstrained lattice constant with higher Si concentration. Notice, however, that the $Fe_{0.76}Si_{0.24}$ lattice is still expanded compared to GaAs at a composition very close to that of the Heusler compound Fe_3Si. Interestingly, the thickness oscillations [Fig. 4(a)] are weaker than that of the corresponding $Fe_{0.84}Si_{0.16}$ film, although HRTEM [Fig. 4(b)] still seems to indicate the formation of a sharp interface (see below). We remark that the interface to the vacuum investigated by AFM exhibits a root mean square (rms) roughness smaller than 0.5 nm for all films.

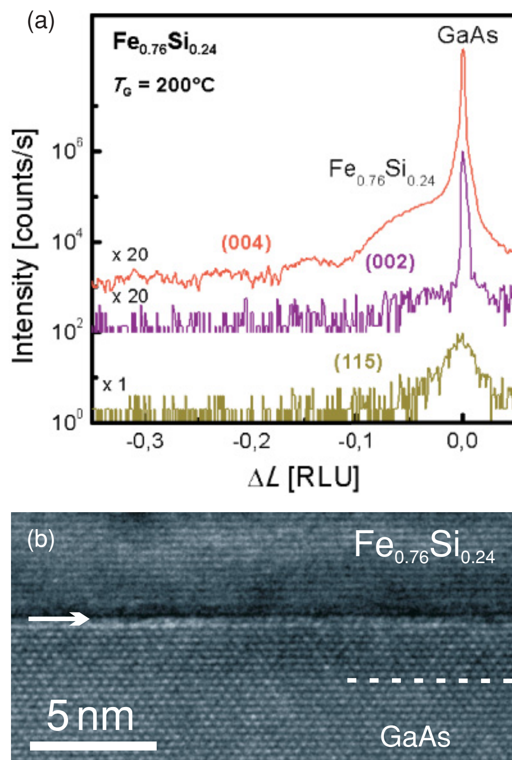

FIG. 4. (Color online) (a) XRD spectra (intensity versus relative x-ray momentum change in reciprocal lattice units) along specific superlattice reflections of a $Fe_{0.76}Si_{0.24}$ film deposited at 200° onto GaAs(001). Note that particularly the intensity of the (115) reflection is very low, where even for the GaAs(115) peak less than 10 counts/s are detected (compared to 10^4 counts/s for the GaAs(004) peak). (b) Corresponding HRTEM images along [110] of the interface region of $Fe_{0.76}Si_{0.24}$/GaAs(001); dashed line indicates affected region in the GaAs substrate (see text).

As discussed by Jenichen *et al.*,[15] the intensity of specific XRD superlattice reflections provides insight into the crystallographic ordering of the films. $Fe_{1-x}Si_x$ is a binary ferromagnetic alloy that crystallizes in the $D0_3$ structure for the Heusler compound Fe_3Si (i. e., $x = 0.25$). The $D0_3$ lattice consists of a regular array of body-centered cubes where the corners (A and C in Fig. 1) are occupied by Fe atoms and the center atom is alternatingly Fe (B) or Si (D). For lower and higher Si concentrations the bcc lattice sites inherently are occupied more and more at random by Fe and Si leading to a disappearance of the (002) and (115) reflections. Indeed we detect no intensity at the angles of the (002) and (115) planes for the $Fe_{0.84}Si_{0.16}$ films (not shown) in agreement with Ref. 15. In the case of the $Fe_{0.76}Si_{0.24}$ film, on the other hand, both reflections are observed [Fig. 4(a)]. The former confirms a filling of the pure Fe planes of the $D0_3$ lattice (A and C in Fig. 1) preferentially by Fe atoms, the latter appears only when the Fe/Si planes are atomically ordered (B and D in Fig. 1). Compared to the 30-nm films investigated in Ref. 15, the superlattice reflections of our 7-nm films are significantly weaker and remain weak even when measured with intense synchrotrone x-ray sources. The reduced crystallographic order may be explained by the dominant role of interdiffusion observed in the thin films (see in the following).

B. Magnetic properties

The excellent structural quality of our films is further corroborated by the magnetic properties. Magnetic hysteresis loops measured quantitatively at room temperature with the *in situ* CBM are displayed in Fig. 5; the magnetic field was ramped along the [110] direction. Consistent with the results of Ref. 13, the coercive fields particularly of the 150 °C and 200 °C films are extremely low ($H_c < 0.15$ mT), thus confirming the absence of defects which may act as pinning centers for domain-wall motion. For the 250 °C film the coercive field is still low ($H_c \sim 1.0$ mT) but already significantly larger than at lower T_G, which—in agreement with the HRTEM results of Fig. 2(c)—indicates a degrading of the film structure. As discussed in more detail in Sec. III F, the saturation magnetization values (Table I) are in good agreement with literature results. It is noteworthy that the [110] direction is not an easy magnetization axis of the $Fe_{1-x}Si_x$ films.[13] A close inspection of Fig. 5 reveals that for $T_G < 250\,°C$ the hysteresis loops are not square shaped but exhibit a remanence magnetization well below the saturation magnetization (M_s). In agreement with Lenz *et al.*[14] the easy magnetization axes are directed along [100] and [010]. Due to a small uniaxial anisotropy field the symmetry between the two in-plane ⟨110⟩ hard axes is broken, thereby transforming the [110] direction to a weak intermediate axis.

C. Film stress

Figure 6 shows the evolution of the film forces (F/w) of various $Fe_{0.84}Si_{0.16}$ films normalized to unit film width (w) as a function of the nominal mean film thickness (t) determined by

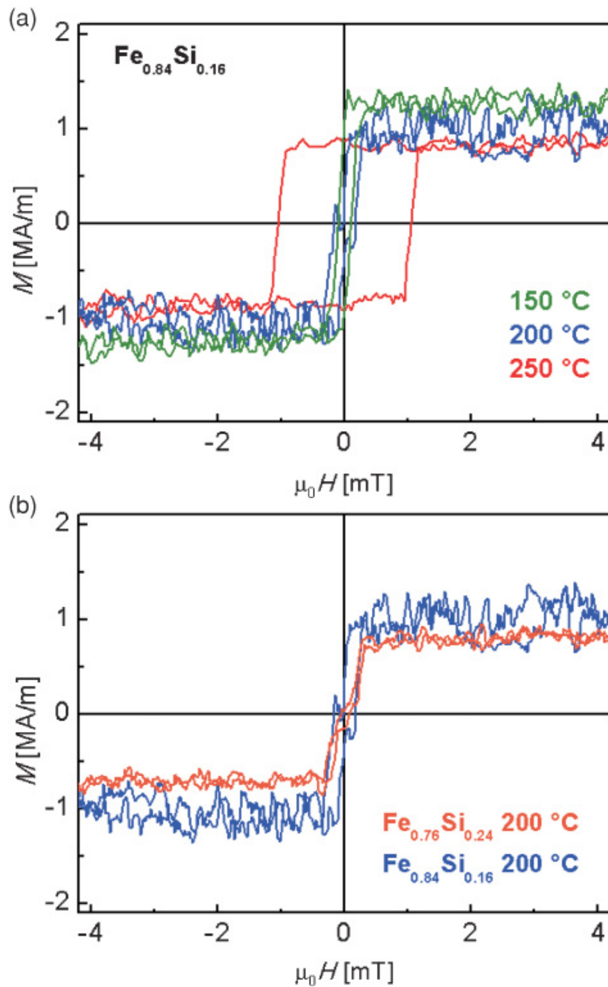

FIG. 5. (Color online) Magnetic hysteresis loops (magnetization M versus magnetic field $H \parallel [110]$) of $Fe_{1-x}Si_x$/GaAs(001) measured at room temperature: (a) $Fe_{0.84}Si_{0.16}$ films deposited at 150 °C, 200 °C, and 250 °C. (b) $Fe_{0.76}Si_{0.24}$ films deposited at 200 °C in comparison with the respective $Fe_{0.84}Si_{0.16}$ film.

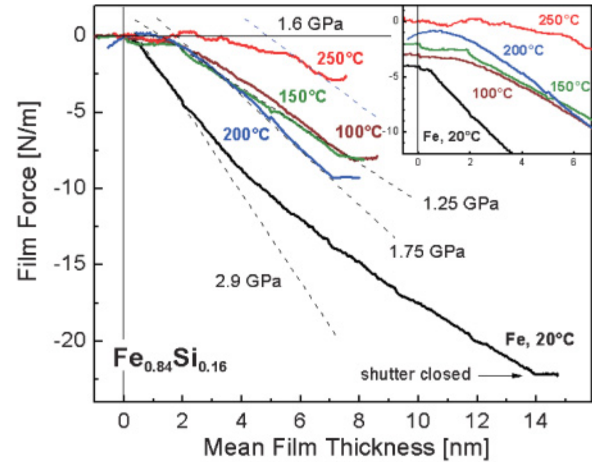

FIG. 6. (Color online) Film force (force per unit film width as a function of the mean film thickness) evolving during and after MBE growth of various $Fe_{0.84}Si_{0.16}$ films deposited onto GaAs(001) at 100 °C, 150 °C, 200 °C, and 250 °C. For comparison, the force curve of a pure Fe film deposited at room temperature is included; slope of dashed lines corresponds to indicated film stress. Film force curves in the inset are subsequently displaced by 1N/m to enable a better view on the respective induction periods.

QCM. All force curves exhibit an induction period extending over a thickness of 2–3 nm as well as linearly increasing compressive forces at higher film thickness. Linearly increasing film forces correspond to constant incremental film stress ($F/w = \sigma t$). For comparison, Fig. 6 includes also a force curve of a pure Fe film ($x = 0$) deposited at room temperature. For pure Fe the induction period ends already after deposition of 2–3 ML which is the typical thickness range for surface- and interface-stress effects to dominate. At higher thicknesses the stress is governed by the misfit strain between the lattices of GaAs and Fe. The dashed line in Fig. 6 corresponds to the film forces due to misfit strain of 1.38% calculated by the bulk lattice constants $a_{GaAs} = 0.5653$ nm and $2 \times a_{Fe} = 0.5732$ nm. Its slope—corresponding to 2.9 GPa—is in perfect agreement with that of the experimental force curve up to a thickness of about 2–3 nm at which part of the strain is relieved by misfit dislocations.

With increasing Si content ($x > 0$) the lattice constant of $Fe_{1-x}Si_x$ films decreases and nearly matches with that of GaAs at the composition of the Heusler compound Fe_3Si ($a_{Fe_3Si} = 0.5655$ nm[18]). For the $Fe_{0.84}Si_{0.16}$ films misfit-induced compressive stress of 1.23–1.38 GPa should be expected (σ^T_{mf} in Table I). Compressive stress indeed is measured experimentally, but only after an induction period of 2–3 nm. At $T_G = 100$ and 150 °C the magnitude of the experimental compressive stress (σ^T_{exp} in Table I) is in very good agreement with the bulk misfit stress. At higher T_G, however, σ^T_{exp} exceeds σ^T_{mf} significantly. At lower thickness the stress is weakly compressive or even tensile. Compared with the room-temperature Fe film, the thickness range of the induction period of the $Fe_{1-x}Si_x$ films is decisively increased, from 2–3 ML to 15 ML for $T_G = 100$ and 150 °C, to 20 ML for $T_G = 200$ °C and to 30 ML for $T_G = 250$ °C (inset of Fig. 6). Thus the range of surface- and interface-stress related effects is exceeded by far. Furthermore, strain relief by misfit dislocations can be definitely ruled out. HRTEM reveals perfect pseudomorphic growth up to the maximum deposited thickness of ∼7 nm consistent with constant stress (indicated by dashed lines in Fig. 6, i.e., no kinks). Moreover, in azimuthal XRD scans only GaAs peaks are observed, thus confirming that the in-plane lattice spacing of GaAs(001) is transmitted without interruption into the entire growing film. These results therefore imply that the compressive misfit stress is not relieved, but rather compensated by the tensile stress contributions of other processes. Figure 7 depicts the film forces of a $Fe_{0.76}Si_{0.24}$ film deposited at 200 °C. For this film the stress developing during the induction period is tensile and becomes compressive at a mean thickness of about 2 nm. Compared with the $Fe_{0.84}Si_{0.16}$ films the measured compressive stress has decreased to 0.85 GPa, but again it is considerably larger than the calculated misfit stress (Table I). We remark that Fe deposition at 200 °C is accompanied by strong interdiffusion of Fe into GaAs and Ga and As into the Fe film, reflected also by the stress behavior (for details see Ref. 19 and references therein).

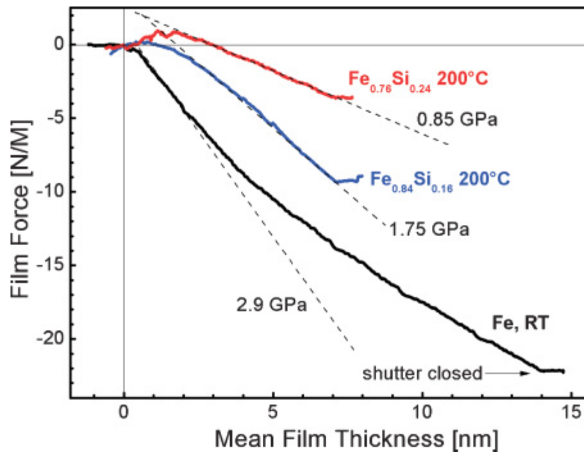

FIG. 7. (Color online) Film force (force per unit film width as a function of the mean film thickness) evolving during and after MBE growth of an $Fe_{0.76}Si_{0.24}$ film deposited onto GaAs(001) at 200 °C. For comparison, also the force curves of a respective $Fe_{0.84}Si_{0.14}$ film and a pure Fe film deposited at room temperature are included. Dashed lines indicate the film forces evolving due to the maximum misfit stress calculated by bulk lattice constants.

D. AES depth profiling

In order to further elucidate interdiffusion in $Fe_{1-x}Si_x$/GaAs(001) as suggested by the stress experiments we investigated the 200° $Fe_{0.76}Si_{0.24}$ film by AES depth profiling. Figure 8 displays the relative atomic concentrations of Fe, Si, As, Ga, and O of the surface layer while milling it by Ar sputtering, thus reflecting the depth distribution of these elements. The peaks appearing in the Fe and Si plots at the beginning of Ar sputtering coincide with the maximum in the oxygen plot and originate from a 1–2-nm thick oxide layer due to air exposure of the sample. Upon further milling the signals of Fe and Si become constant and start decaying after about 50 sputtering cycles. At the same time the signals of As and Ga begin to rise. Obviously, the rise of the Fe and Si signals proceeds with a much larger slope than their decay (compare with dotted line in Fe plot), thus indicating a gradual rather than an abrupt decrease of the atomic concentration. The AES signals of As and Ga, on the other hand increases gradually with a small slope. Taking the two findings together, points to the formation of an intermixed layer at the interface, where all four elements, Fe, Si, As, and Ga, are coexisting. Note the remaining small oxygen signal (<5%) up to about 65 sputtering cycles. It can be explained either by a minor oxidation of the $Fe_{0.76}Si_{0.24}$ bulk because of air exposure of the sample or by always anew oxide formation at the sputtered surface due to oxygen impurity of the Ar sputtering gas (see Ref. 8). Since the residual oxygen signal is coupled to the presence of a film layer, its disappearance (dashed line in Fig. 8) enables a thickness calibration of the abscissa of Fig. 8 and provides an estimate of the thickness of the intermixed layer (2–3 nm in both film and substrate). Finally we want to remark, that As diffusion into the $Fe_{0.76}Si_{0.24}$ film is confirmed by the small peak at about 10 sputtering cycles in the As plot. It lies near the surface of the as-deposited film (i.e., beneath the surface oxide after air exposure), and indicates surface segregation of As during growth analogous to Fe/GaAs(001).[20]

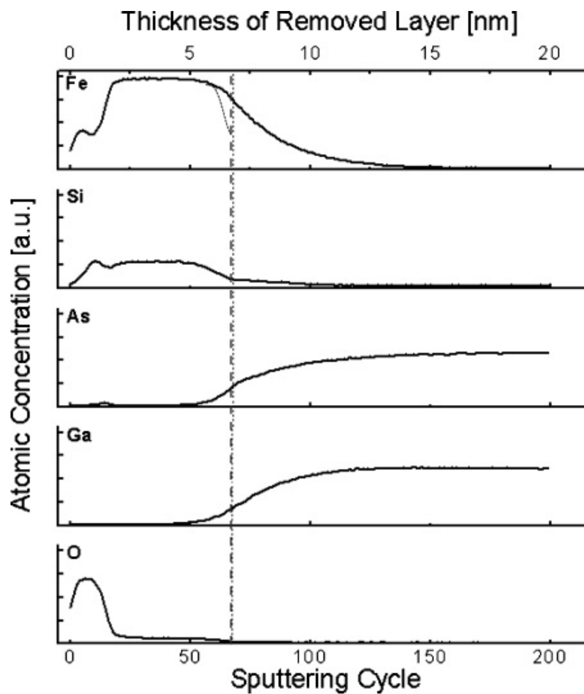

FIG. 8. Auger depth profiles of Fe, Si, As, Ga, and O of the $Fe_{0.76}Si_{0.24}$ film deposited at 200 °C onto GaAs(001); dashed line marks the lower film end as indicated by the disappearance of the oxygen signal and used for thickness calibration (upper scale), the expected decay of the Fe signal in the case of a sharp interface, and the kink in the Si signal.

E. EDX spectroscopy

In order to gain a more detailed insight into the diffusion profiles of the four participating elements, STEM-EDXS investigations were performed on both film types as shown in Fig. 9. The distance between subsequent measuring points of the linescans across the GaAs/$Fe_{1-x}Si_x$ interface was 0.4 nm [see insets of Figs. 9(a) and 9(b)]. Figure 9 corroborates the AES depth-profiling results previously mentioned that Fe and Si are diffused into the GaAs substrate and Ga and As into the $Fe_{1-x}Si_x$ films. The zone of pronounced interdiffusion has a total width of about 5 nm in both specimens with Fe diffusing more strongly than Si, and Ga more strongly than As (compare normalized spectra; Fig. 9, right). At a distance of about 4 nm away from the interface the concentration of all components has converged to the expected bulk values as indicated by the EDX spectra of Fig. 9 (left), which have been quantified by the k-factor method.[21] In the GaAs substrate, weak stray signals of Fe, Co, and Si originating from the microscope itself were recorded at higher distances.

F. Discussion

This section provides a comparative discussion of the results obtained by the different experimental techniques. The main finding of this study certainly is the discovery of a broad intermixed region at the interface between the $Fe_{1-x}Si_x$ films and the GaAs(001) substrate that forms already at temperatures necessary for the crystallographic ordering of Heusler films.

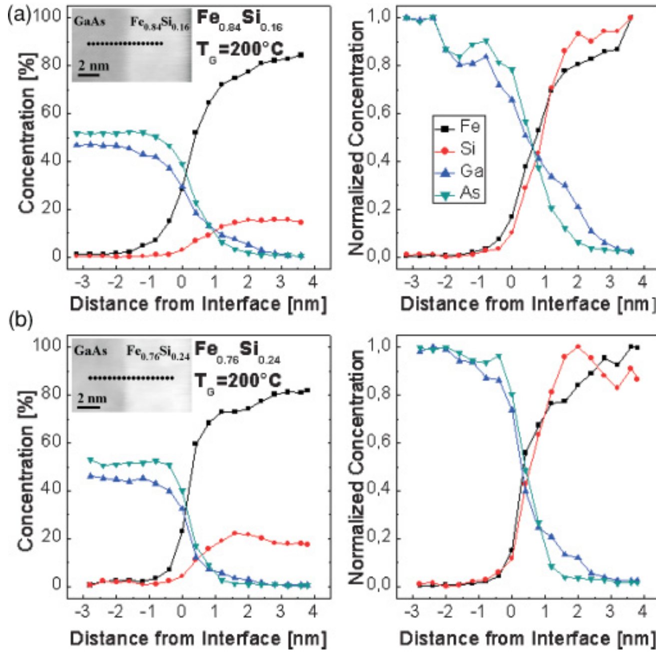

FIG. 9. (Color online) Quantified (left) and normalized (right) STEM-EDXS linescans of Fe, Si, Ga, and As in (a) $Fe_{0.84}Si_{0.16}$/GaAs(001) and (b) $Fe_{0.76}Si_{0.24}$/GaAs(001), both deposited at 200 °C; insets show the positions at which the EDX spectra were taken.

Film stress. Whereas XRD and HRTEM indicate pseudomorphic growth up to the total deposited film thickness (∼7 nm), the stress measurements reveal an induction period at the beginning of film growth with a thickness of 2–5 nm depending on the growth temperature (t_{ind} in Table II). During this growth stage only weak compressive stress that is significantly smaller than the respective misfit stress (σ_{mf}; see Table I), or even tensile stress is observed. This result is indeed surprising as pseudomorphic growth conserves the information of the substrate lattice distance. Accordingly, the misfit strain cannot be relieved during the induction period, but is rather compensated by a tensile stress contribution. A very

TABLE I. Bulk misfit stress σ_{mf}^T, experimental stress σ_{exp}^T, and the biaxial elastic constant E_{biax}^T calculated by Eq. (1) as well as the experimental saturation magnetization M_s and coercive field $\mu_0 H_c$ of various $Fe_{1-x}Si_x$ films deposited at different growth temperatures T_G.

$Fe_{1-x}Si_x$	T_G [°C]	σ_{mf}^T [GPa]	σ_{exp}^T [GPa]	E_{biax}^T [GPa]	M_s [MA/m]	H_c [mT]
$Fe_{0.84}Si_{0.16}$	20	−1.23		190		
$Fe_{0.84}Si_{0.16}$	100	−1.27	−1.25	182	1.3	–
$Fe_{0.84}Si_{0.16}$	150	−1.31	−1.25	178	1.3	0.15
$Fe_{0.84}Si_{0.16}$	200	−1.36	−1.75	173	1.1	0.10
$Fe_{0.84}Si_{0.16}$	250	−1.38	−1.60	168	0.9	1.0
$Fe_{0.76}Si_{0.24}$	20	−0.19		179		
$Fe_{0.76}Si_{0.24}$	200	−0.37	−0.85	163	0.85	0.1

[a]the elastic constants c_{11} and c_{12} for the calculation of E_{biax}^T were obtained by interpolation between the temperature-dependent elastic constants of Fe_3Si and Fe from Ref. 22.

TABLE II. Comparison of film thickness t determined by QCM, XRD, and TEM of various $Fe_{1-x}Si_x$ films deposited at different growth temperatures T_G as well as the respective thickness t_{ind} of the induction period in the film force curves.

$Fe_{1-x}Si_x$	T_G (°C)	t_{QCM} (nm)	t_{XRD} (nm)	t_{TEM} (nm)	t_{ind} (nm)
$Fe_{0.84}Si_{0.16}$	100	7.6 ± 0.2	–	–	2.0
$Fe_{0.84}Si_{0.16}$	150	7.2 ± 0.2	7.6 ± 0.1	7.3 ± 0.2	2.0
$Fe_{0.84}Si_{0.16}$	200	7.0 ± 0.2	7.2 ± 0.1	6.9 ± 0.2	2.2
$Fe_{0.84}Si_{0.16}$	250	7.0 ± 0.2	6.6 ± 0.1	6.3 ± 0.5	∼5
$Fe_{0.76}Si_{0.24}$	200	7.1 ± 0.2	7.0 ± 0.1	7.3 ± 0.2	2.0

likely mechanism that generates tensile stress is interdiffusion. It is not immediately detectable by HRTEM and XRD but clearly evidenced by AES depth profiling and STEM-EDXS, which indicate 2–3-nm thick regions in both film and substrate, where Fe, Si, As, and Ga coexist. As proposed in a previous study of Fe(001)/GaAs(001),[9] tensile stress arises when As or Ga atoms diffuse out of the GaAs matrix and leave voids behind. A net tensile stress remains, even when the voids are refilled by Fe (or here also Si), since the volume of these atoms is smaller compared to Ga or As. Transferring this mechanism to $Fe_{1-x}Si_x$/GaAs(001) suggests that the "induction period" of the $Fe_{1-x}Si_x$ films is dominated by site exchange processes that do not affect the crystal structure of film and substrate but lead to an intermixed interface region with a reduced net compressive stress. In fact, in the HRTEM image of the $Fe_{0.76}Si_{0.24}$ film a 2–3-nm wide region in the GaAs can be recognized [marked by a dashed line in Fig. 4(b)] that exhibits a darker contrast and may indicate a layer of different strain and/or composition. Furthermore, a clearly disturbed interface region is imaged for the 250 °C $Fe_{0.84}Si_{0.16}$ film [Fig. 2(c)], where additionally also the local crystallographic structure is disturbed (e.g., due to the formation of precipitates). On the other hand, diffusion via interstitial sites leads to compressive stress. This diffusion mechanism seems to dominate in thicker films prepared at $T_G > 150$ °C, which explains the higher compressive stress in the $Fe_{0.84}Si_{0.16}$ and $Fe_{0.76}Si_{0.24}$ films compared with the misfit stress calculated with the lattice constants of respective bulk compounds (Table I).

Magnetic properties. As discussed in Sec. III B and consistent with Lenz *et al.*[14] the easy magnetization axes of our $Fe_{1-x}Si_x$ films are directed along [100] and [010]; $[\bar{1}10]$ and [110] are in-plane hard and intermediate axes, respectively. The coercive fields (Table I), particularly for growth temperatures between 150 °C and 200 °C, are very low (<1.5 mT), thus corroborating the excellent structural quality of the films. In Table I also the saturation magnetization M_s of the $Fe_{1-x}Si_x$ films is listed. M_s of the $Fe_{0.84}Si_{0.16}$ films lies between 0.9 and 1.3 MA/m with the highest values for the optimum T_G range of 150 °C and 200 °C. Reduced structural order at lower temperatures as well as strong interdiffusion and formation of precipitates at higher temperatures may explain the decrease in M_s. Taking the magnetic moments of an *ab initio* study of Kudrnovsky *et al.*[23] and extrapolating them for $Fe_{0.84}Si_{0.16}$ one obtains $\mu_{\mathrm{Fe(A,C)}} = 1.51\mu_B$, $\mu_{\mathrm{Fe(B)}} = 2.39\mu_B$, $\mu_{\mathrm{Fe(D)}} = 2.28\mu_B$, and $\mu_{\mathrm{Si(D)}} = -0.10\mu_B$. With these values a saturation magnetization of 1.25 MA/m is calculated, which is

in good agreement with the experimental values. For comparison, Zareki *et al.*[24] report a value of 1.03 MA/m for an 8-nm thick $Fe_{0.80}Si_{0.20}$ film deposited at 210 °C onto MgO(001) and annealed at 630 °C for one hour. M_s of the $Fe_{0.76}Si_{0.24}$ film deposited at 200 °C, which is crystallographically ordered according to the $D0_3$ lattice, is 0.85 MA/m. This value is in good agreement with recent experimental (1.02 MA/m,[25] 0.74 MA/m,[26] 0.79 MA/m,[14] 0.88 MA/m[24]) and theoretical studies (0.11 MA/m[23]).

Film thickness. Commonly, in III/V MBE the thickness of thin films and heterostructures is determined *ex situ* by evaluating respective thickness oscillations in XRD spectra. In the present study three independent experimental techniques have been employed: (i) XRD which senses the thickness of crystallographically ordered phases, (ii) HRTEM which can distinguish different phases in real space, and (iii) QCM which measures the mass equivalent of the deposited components (Fe and Si) from which the thickness of the deposited alloy film can be calculated. The film thickness obtained by the three methods (see Table II) agrees well within experimental error except for the 250 °C film with a broad interface region due to parallel interface reactions. In all other cases a significant "material loss" due to unidirectional diffusion of film atoms into the substrate can be excluded. Diffusion proceeds in both directions and is rather an exchange of atoms.

Comparison XRD/stress measurements. It is worth comparing the results obtained by the two complementary techniques, XRD and stress measurements, as both methods yield values of the unstrained lattice constant a_0^{RT} of the $Fe_{1-x}Si_x$ films.

Hooke's law relates biaxial stress σ in the (100) plane of a cubic lattice to respective strain $\epsilon_{(100)}$ by $\sigma_{\text{exp}} = E_{\text{biax}}\epsilon_{(100)}$. E_{biax} is the elastic constant for biaxial stress:

$$E_{\text{biax}} = \frac{(c_{11} - c_{12})(c_{11} + 2c_{12})}{c_{11}}. \quad (1)$$

Temperature-dependent values E^T_{biax} calculated by interpolation between the temperature-dependent elastic constants, c_{11} and c_{12}, of Fe_3Si and Fe from Ref. 22 are listed in Table I. From $\epsilon_{(100)} = (a - a_0)/a_0^T$ one obtains

$$a^T_{0,\text{exp}} = \frac{a^T}{1 + \epsilon^T_{(100)}} = \frac{a^T_{\text{GaAs}}}{1 + \sigma^T_{\text{exp}}} \bigg/ E^T_{\text{biax}}. \quad (2)$$

$a^T_{0,\text{exp}}$ is the unstrained lattice constant of the $Fe_{1-x}Si_x$ films at the temperature T; a^T is the strained lattice constant at the temperature T with $a^T = a^T_{\text{GaAs}}$ (pseudomorphic growth!), the respective unstrained lattice constant of the GaAs(001) plane, all listed in Table III. For $T_G = 100$ °C and 150 °C, $a^T_{0,\text{exp}}$ agrees perfectly with the respective bulk lattice constants $a^T_{0,\text{bulk}}$; at higher temperatures $a^T_{0,\text{exp}}$ is slightly, but significantly expanded.

The values discussed so far refer always to the respective growth temperature, whereas the XRD experiments were performed at room temperature (RT). In order to transform the unstrained lattice constants $a^T_{0,\text{exp}}$ of the $Fe_{1-x}Si_x$ films to room temperature, we use a thermal expansion $\alpha = 1.38 \times 10^{-5}$ K^{-1} derived from the temperature-dependent bulk lattice constants of Ref. 18. The obtained values are listed in Table III as $a^{RT}_{0,\text{exp}}$. Whereas at $T_G = 100$ °C and 150 °C these values agree nicely with the room-temperature bulk value of 0.5690 nm, they again differ slightly at higher T_G.

TABLE III. Temperature-dependent lattice constants of $Fe_{0.84}Si_{0.16}$, $Fe_{0.76}Si_{0.24}$, and GaAs(001) for the different growth temperatures T_G: $a^T_{0,\text{bulk}}$, bulk values from Ref. 18; $a^T_{0,\text{exp}}$, unstrained lattice constants derived from the experimental stress of Figs. 6 and 7 via Eq. (2); $a^{RT}_{0,\text{exp}}$, respective unstrained values at room temperature calculated from $a^T_{0,\text{exp}}$ with a thermal expansion coefficient $\alpha = 1.38 \times 10^{-5}$ K^{-1};[a] $a^{RT}_{0,\text{XRD}}$, unstrained in-plane lattice constant calculated from the XRD data by Eq. (3); $a^T_{0,\text{GaAs}}$, temperature-dependent lattice constants of GaAs(001) calculated with a thermal expansion coefficient $\alpha = 6.2 \times 10^{-6}$ K^{-1}.

$Fe_{1-x}Si_x$	T_G [°C]	$a^T_{0,\text{bulk}}$ [nm]	$a^T_{0,\text{exp}}$ [nm]	$a^{RT}_{0,\text{exp}}$ [nm]	$a^{RT}_{0,\text{XRD}}$ [nm]	$a^T_{0,\text{GaAs}}$ [nm]
$Fe_{0.84}Si_{0.16}$	20	0.5690				0.5653
$Fe_{0.84}Si_{0.16}$	100	0.5696	0.5695	0.5689		0.5656
$Fe_{0.84}Si_{0.16}$	150	0.5700	0.5698	0.5688	0.5702	0.5658
$Fe_{0.84}Si_{0.16}$	200	0.5704	0.5717	0.5703	0.5707	0.5659
$Fe_{0.84}Si_{0.16}$	250	0.5708	0.5715	0.5697	0.5710	0.5661
$Fe_{0.76}Si_{0.24}$	20	0.5659				0.5653
$Fe_{0.76}Si_{0.24}$	200	0.5672	0.5689	0.5675	0.5687	0.5659

[a]calculated from the bulk lattice constants of Ref. 18.

$a^T_{0,\text{XRD}}$, on the other hand, is obtained by XRD which measures precisely the in-plane and out-of-plane lattice distances of thin films. Evaluating the relation $\epsilon_{(001)} = -c_{11}/(2c_{12})\epsilon_\perp$ with $\epsilon_{(001)}$ being the biaxial strain implied by the substrate one obtains

$$a^{RT}_{0,\text{XRD}} = \frac{a^{RT}_{\perp,\text{XRD}} + (2c_{12}/c_{11})\, a^{RT}_{0,\text{GaAs}}}{1 + 2c_{12}/c_{11}}. \quad (3)$$

$2c_{12}/c_{11} = 1.27$ for $Fe_{0.84}Si_{0.16}$ and 1.33 for $Fe_{0.76}Si_{0.24}$ (from Ref. 22). The good agreement between $a^{RT}_{0,\text{exp}}$ and $a^{RT}_{0,\text{XRD}}$, both listed in Table III, confirms the consistency between XRD and the stress experiments.

$Fe_{1-x}Si_x$ composition. In the present study the amount of deposited material, Fe and Si, is measured during the film preparation by QCM. We estimate the absolute error of our setup to be about 3%, the relative error of the two sources—relevant for composition—even smaller. The film composition deduced from the QCM data is confirmed by the stress measurements as a further *in situ* technique. For the $Fe_{0.84}Si_{0.16}$ films deposited at 100 °C and 150 °C, the derived lattice constants of the unstrained films are in nearly perfect agreement with the respective bulk values of Lihl and Ebel[18] for film concentrations of 16%. For higher T_G ($\geqslant$200 °C) the experimental stress is (significantly) larger than the respective misfit stress. Ignoring other stress mechanisms, the stress results would indicate a decrease of the Si concentration to 13.2%, which contradicts enhanced Fe diffusion indicated by AES depth profiling and STEM-EDXS. Instead, diffusion proceeds preferentially via interstial sites which gives rise to additional compressive stress. The stress investigations therefore demonstrate the difficulty of determining the composition of a multicomponent system, where other stress mechanisms in addition to misfit contribute to the total stress. *Ex situ* investigations by XRD confirm the stress results. It should be emphasized, however, that also for XRD detailed knowledge

of the origin of the strain state is required for determining composition, since processes other than misfit may modify the unstrained lattice distance. Only when exclusively misfit stress is involved and the film is thick enough for the elastic constants to be bulklike, the unstrained lattice constant can be calculated from the in-plane and out-of-plane lattice constants of the film and compared with respective bulk values if available.

IV. CONCLUSION

We have investigated the role of interdiffusion in MBE of the binary Heusler alloy system $Fe_{1-x}Si_x$/GaAs(001), employing a variety of complementary techniques: (i) *in situ* stress measurements, (ii) QCM, (iii) x-ray diffraction (XRD), (iv) HRTEM, (v) RHEED, LEED, and AFM, (vi) CBM, (vii) AES depth profiling, and (viii) STEM-EDXS. The main properties of the investigated $Fe_{0.84}Si_{0.16}$ and $Fe_{0.76}Si_{0.24}$ films—growth, epitaxy, crystallographic order, interface quality, saturation magnetization, coercive field, and magnetic anisotropy—are in perfect agreement with the literature. In their combination, our complementary experimental techniques reveal a strong interdiffusion of Fe and Si into the GaAs substrate as well as of As and Ga into the $Fe_{1-x}Si_x$ films, creating intermixed layers of 2–3-nm thickness in both film and substrate. Interdiffusion is dominant already at moderate growth temperatures required for crystallographic ordering. These findings are not contradictory to previous work. Interdiffusion effects rather have escaped detection by the established, typically *ex situ* characterization techniques of semiconductor research which are not particularly sensitive to interface composition. We remark that the presence of an intermixed interface region of a few nanometers may explain the low spin-injection efficiency ($<3\%$) detected in Fe_3Si/GaAs(001) by a light-emitting-diode configuration,[27] although the spin polarization of Fe_3Si is similar to Fe ($\sim45\%$) as found by Andreev reflection[16] and predicted by theory.[28–30] In view of our alarming results, future work on ferromagnet/semiconductor hybrid systems needs to focus on the development of appropriate barrier layers inhibiting diffusion that is detrimental for the properties of both ferromagnet and semiconductor.

ACKNOWLEDGMENTS

We thank J. Herfort, O. Brandt, and M. Arndt for helpful discussions, B. Sepiol for providing the lattice-distance data, as well as the Austrian Fonds zur Förderung der Wissenschaftlichen Forschung (Project No. P20650) and the German BMBF under the research program NanoQUIT (Contract No. 01BM463) for financial support.

[1] S. Datta and B. Das, Appl. Phys. Lett. **56**, 665 (1990).
[2] A. Ney, C. Pampuch, R. Koch, and K. H. Ploog, Nature (London) **425**, 485 (2003).
[3] S. S. P. Parkin, C. Kaiser, A. Panchula, P. M. Rice, B. Hughes, M. Samant, and S.-H. Yang, Nat. Mater. **3**, 862 (2004).
[4] D. Orgassa, H. Fujiwara, T. C. Schulthess, and W. H. Butler, Phys. Rev. B **60**, 13237 (1999).
[5] B. Hülsen, M. Scheffler, and P. Kratzer, Phys. Rev. Lett. **103**, 046802 (2009).
[6] M. Ramsteiner, O. Brandt, T. Flissikowski, H. T. Grahn, M. Hashimoto, J. Herfort, and H. Kostial, Phys. Rev. B **78**, 121303(R) (2008).
[7] M. Hashimoto, J. Herfort, A. Trampert, H.-P. Schönherr, and K. H. Ploog, J. Vac. Sci. Technol. B **24**, 2004 (2006).
[8] R. Koch, Surf. Coat. Technol. **204**, 1973 (2010).
[9] G. Wedler, B. Wassermann, R. Nötzel, and R. Koch, Appl. Phys. Lett. **78**, 1270 (2001).
[10] M. Weber, R. Koch, and K.-H. Rieder, Phys. Rev. Lett. **73**, 1166 (1994).
[11] S. H. Liou, S. S. Malhotra, J. X. Shen, M. Hong, J. Kwo, H. S. Chen, and J. P. Mannaerts, J. Appl. Phys. **73**, 6766 (1993).
[12] J. Herfort, H.-P. Schönherr, and K. H. Ploog, Appl. Phys. Lett. **83**, 3912 (2003).
[13] J. Herfort, H.-P. Schönherr, K.-J. Friedland, and K. H. Ploog, J. Vac. Sci. Technol. B **22**, 2073 (2004).
[14] K. Lenz, E. Kosubek, K. Baberschke, H. Wende, J. Herfort, H.-P. Schönherr, and K. H. Ploog, Phys. Rev. B **72**, 144411 (2005).
[15] B. Jenichen, V. M. Kaganer, J. Herfort, D. K. Satapathy, H. P. Schönherr, W. Braun, and K. H. Ploog, Phys. Rev. B **72**, 075329 (2005).
[16] A. Ionescu *et al.*, Phys. Rev. B **71**, 094401 (2005).
[17] J. Herfort, B. Jenichen, V. M. Kaganer, A. Trampert, H.-P. Schönherr, and K. H. Ploog, Physica E **32**, 371 (2006).
[18] F. Lihl and H. Ebel, Archiv für Eisenhüttenwesen **32**, 489 (1961).
[19] T. Ashraf, C. Gusenbauer, J. Stangl, G. Hesser, M. Wegscheider, and R. Koch, J. Phys.: Condens. Matter **23**, 042001 (2011).
[20] S. A. Chambers, F. Xu, H. W. Chen, I. M. Vitomirov, S. B. Anderson, and J. H. Weaver, Phys. Rev. B **34**, 6605 (1986).
[21] O. Eibl, Ultramicroscopy **50**, 179 (1993).
[22] J. B. Rausch and F. X. Kayser, J. Appl. Phys. **48**, 487 (1977).
[23] J. Kudrnovsky, N. E. Christensen, and O. K. Andersen, Phys. Rev. B **43**, 5924 (1991).
[24] K. Zakeri, S. J. Hashemifar, J. Lindner, I. Barsukov, R. Meckenstock, P. Kratzer, Z. Frait, and M. Farle, Phys. Rev. B **77**, 104430 (2008).
[25] V. A. Niculescu, T. J. Burch, and J. I. Budnick, J. Magn. Magn. Mater. **39**, 223 (1983).
[26] A. Ionescu, C. A. F. Vaz, T. Trypiniotis, C. M. Gürtler, M. E. Vicker, H. Garcia-Miquel, and J. A. C. Bland, J. Magn. Magn. Mater. **286**, 72 (2005).
[27] A. Kawaharazuka, M. Ramsteiner, J. Herfort, H.-P. Schönherr, H. Kostial, and K. H. Ploog, Appl. Phys. Lett. **85**, 3492 (2004).
[28] E. G. Moroni, W. Wolf, J. Hafner, and R. Podloucky, Phys. Rev. B **59**, 12860 (1999).
[29] A. Bansil, S. Kaprzyk, P. E. Mijnarends, and J. Tobola, Phys. Rev. B **60**, 13396 (1999).
[30] N. I. Kulikov, D. Fristot, J. Hugel, and A. V. Postnikov, Phys. Rev. B **66**, 014206 (2002).